4 Electronic Structure of Condensed Matter

4-1 Strong Antiferromagnetic Effects in the Electron-Doped High-Temperature Superconductor $Sm_{2-x}Ce_xCuO_4$

In high-T_c superconductors (HTSCs), superconductivity competes with various ground states. Above all, antiferromagnetic order appears to be the most likely competing ground state irrespective of whether the doped carriers are holes or electrons [1,2]. In order to understand the origin and mechanism of superconductivity in HTSCs, it is important to elucidate the interplay between superconductivity and antiferromagnetism. For direct observation of their interplay, it is necessary to investigate the electronic structure associated with both phenomena. In the electron-doped HTSCs $Ln_{2-x}Ce_xCuO_4$ (Ln = La, Pr, Nd, Sm), the superconducting phase is adjacent to or overlaps with the antiferromagnetic phase. Among these materials, $Sm_{2-x}Ce_xCuO_4$ is particularly a remarkable material since the superconducting phase is enclosed by the antiferromagnetic phase in the x-T phase diagram, as revealed by μSR measurements [3]. We have performed angle-resolved photoemission spectroscopy (ARPES) of $Sm_{1.85}Ce_{0.15}CuO_4$ (SCCO) (T_c = 16 K, T_N = 115 K) at beamline BL- 28A using an incident photon energy of 55 eV.

Figure 1 shows a plot of the ARPES intensity at the Fermi level (E_F) in SCCO recorded at T ~ 17 K as a function of the two-dimensional wave vector (k_x, k_y), illustrating the Fermi surface. In agreement with previous studies [4,5], no intensity was observed at the "hot spot", which is the intersection of the Fermi surface of the paramagnetic state (solid curve) and the antiferromagnetic Brillouin zone boundary (dotted line) due to the antiferromagnetic correlation.

Figure 2 shows ARPES intensity plots at various momentum cuts in the Brillouin zone shown in the inset. In the nodal cut (F) which contains (π/2, π/2), a clear folding of the paramagnetic band to the antiferromagnetic Brillouin zone was observed, indicating the strong effect of antiferromagnetism. In SCCO, this band folding is strong enough to open an energy gap around the nodal point. This contrasts with the nodal points of $Pr_{0.89}LaCe_{0.11}CuO_4$ and $Nd_{1.85}Ce_{0.15}CuO_4$ [6,7], in which the superconducting and antiferromagnetic phases do not coexist and neither a band folding and a nodal energy gap was observed. We note that the opening of a gap at the nodal point is an unusual phenomenon in that the superconducting gap symmetry of the d-wave in HTSCs suggests that the gap should be closed at the nodal point. At the hot spot, the energy gap is known to

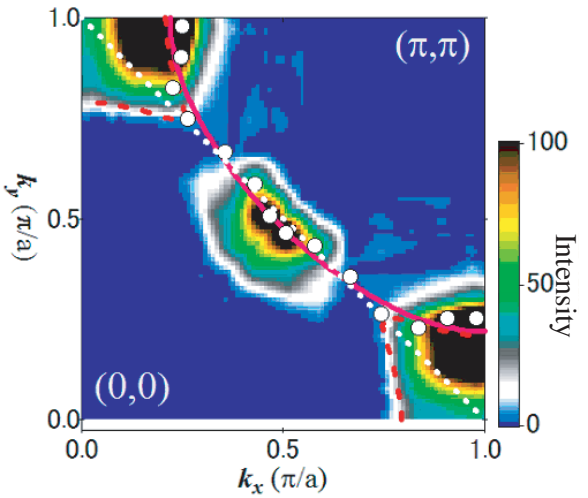

Figure 1
Plot of ARPES intensity at E_F in $Sm_{1.85}Ce_{0.15}CuO_4$ as a function of the two-dimensional wave vector (k_x, k_y). The energy distribution curves have been integrated within a 60 meV window around E_F. The data were recorded over a Brillouin zone octant and symmetrized with respect to the (0,0) to (π, π) line. The white circles are located at the positions of peaks in the momentum distribution curves, indicating the Fermi surface. The white dotted line shows the antiferromagnetic Brillouin zone boundary. The red curves show the Fermi surfaces obtained by tight-binding fits in the paramagnetic state (solid curve) and the antiferromagnetic state (dashed curve).

open due to antiferromagnetic fluctuation. It is possible that the antiferromagnetic fluctuation is strong enough to influence the nodal point and open a gap. Nevertheless, since the largest d-wave superconducting gap opens around (π,0), superconductivity may survive under the presence of such a nodal gap.

In order to quantitatively investigate the effect of antiferromagnetism, we performed a tight-binding fit using the equation

$$E = \varepsilon_0 \pm \sqrt{\Delta^2 + 4t^2\{\cos(k_x a) + \cos(k_y a)\}^2}$$
$$-4t' \cos(k_x a)\cos(k_y a),$$

where t and t' represent transfer integrals between the nearest and the next-nearest-neighbor Cu sites, and ε_0 and Δ the energy of the center of the band and the energy difference between the spin-up and spin-down sites. As shown in Fig. 2, taking into account the effect of the antiferromagnetism produces a better fit. This fit leads to an estimate of the magnitude of the antiferromagnetic gap 2Δ to be 0.14 eV.

In conclusion, we have observed an energy gap with band folding around the nodal point of the electron-doped superconductor SCCO. We consider that the gap is caused by the effects of antiferromagnetism. These observations explain how superconductivity and antiferromagnetism can coexist in electron-doped HTSCs.

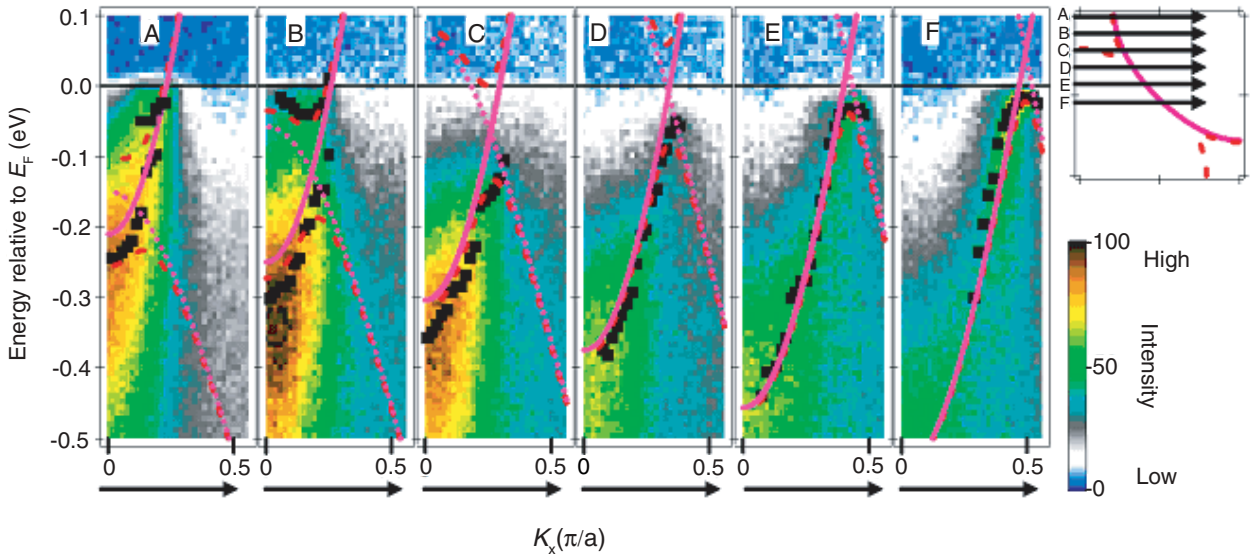

Figure 2
ARPES intensity plots in energy-momentum space at various cuts in the Brillouin zone (inset). Black squares denote the energy-distribution-curve peak positions. The solid and dotted pink curves represent the paramagnetic energy bands and the shadow bands obtained by tight-binding fits. The band of the antiferromagnetic state is represented by a dashed red curve.

M. Ikeda[1], T. Yoshida[1], A. Fujimori[1], M. Kubota[2], K. Ono[2], K. Unozawa[1], T. Sasagawa[1]and H. Takagi[1]
([1]The Univ. of Tokyo, [2]KEK-PF)

References

[1] H. J. Kang, P. Dai, J. W. Lynn, M. Matsuura, J. R. Thompson, S-C. Zhang, D. N. Argyriou, Y. Onose and Y. Tokura, *Nature,* **423** (2003) 522.
[2] B. Lake, H. M. Ronnow, N. B. Christensen, G. Aeppli, K. Lefmann, D. F. Mcmorrow, P. Vorderwisch, P. Smeibidl, N. Mangkorntong, T. Sasagawa, M. Nohara, H. Takagi and T. E. Mason, *Nature*, **415** (2002) 299.
[3] T. Sasagawa *et al.*, *KEK-MSL Report 2005*, (2006) 13.
[4] N. P. Armitage, D. H. Lu, C. Kim, A. Damascelli, K. M. Shen, F. Ronning, D. L. Feng, P. Bogdanov, Z. -X. Shen, Y. Onose, Y. Taguchi, Y. Tokura, P. K. Mang, N. Kaneko and M. Greven, *Phys. Rev. Lett.*, **87** (2001) 147003.
[5] Y. Onose, Y. Taguchi, K. Ishizaka and Y. Tokura, *Phys. Rev. B,* **69** (2004) 024504.
[6] N. P. Armitage, D. H. Lu, D. L. Feng, C. Kim, A. Damascelli, K. M. Shen, F. Ronning, Z. -X. Shen, Y. Onose, Y. Taguchi, and Y. Tokura, *Phys. Rev. Lett.*, **86** (2001) 1126.
[7] H. Matsui, K. Terashima, T. Sato, T. Takahashi, M. Fujita and K. Yamada, *Phys. Rev. Lett.*, **95** (2005) 017003.

4-2 Fermi Surface and Anisotropic Spin-Orbit Coupling of Sb(111) Studied by Angle-Resolved Photoemission Spectroscopy

Group-V semimetals have attracted much attention since they show various interesting physical properties such as quantum size effect [1] and granular superconductivity [2]. To understand the origin of these intriguing behaviors, the band dispersion and the Fermi surface (FS) of Bi(111) surface have been intensively studied by angle-resolved photoemission spectroscopy (ARPES) [3-5], which has revealed that the surface is metallic in contrast to the semimetallic nature of bulk. There have been intensive debates on the spin-split nature of the surface bands and the stability of the surface spin/charge density wave on Bi(111) [4-6]. Clarifying this problem is important not only for understanding the mechanism of anomalous physical properties of group-V semimetal surfaces, but also for opening a way to fabricate new devises based on these peculiar properties [6,7]. A comparative study with Sb, a homologous element with similar structural parameters to those of Bi, would lead to better understanding of the anomalous electronic properties of Bi/Sb-based nanostructure materials.

We have performed high-resolution ARPES at BL-28A as well as at Tohoku University to elucidate the bulk and surface electronic structure of Sb(111) [7]. A clean surface was obtained by *in situ* cleaving along the (111) plane in a vacuum of better than 1×10^{-10} Torr.

Figures 3(a) and (b) show ARPES intensity maps along the $\overline{\Gamma}\,\overline{M}$ direction measured with 65-eV and 73-eV photons. We clearly observe several dispersive bands which are asymmetric with respect to the $\overline{\Gamma}$ point. These bands are ascribed to the bulk Sb 5*p* bands since they show a remarkable photon-energy dependence in the energy position characteristic of the three-dimensional bulk band (see Fig. 3(c)). In addition to these highly dispersive bands, we observe a band near E_F which forms an electron pocket at $\overline{\Gamma}$ point. Since this band does not show a marked photon-energy dependence, it is assigned as a surface band. This assignment is supported by the comparison of experimentally-determined band structure with the band calculation shown in Fig. 3(d), where the experimental band near E_F is situated outside the projection of bulk bands.

To elucidate the origin of the surface band near E_F, we performed ARPES measurements with a higher

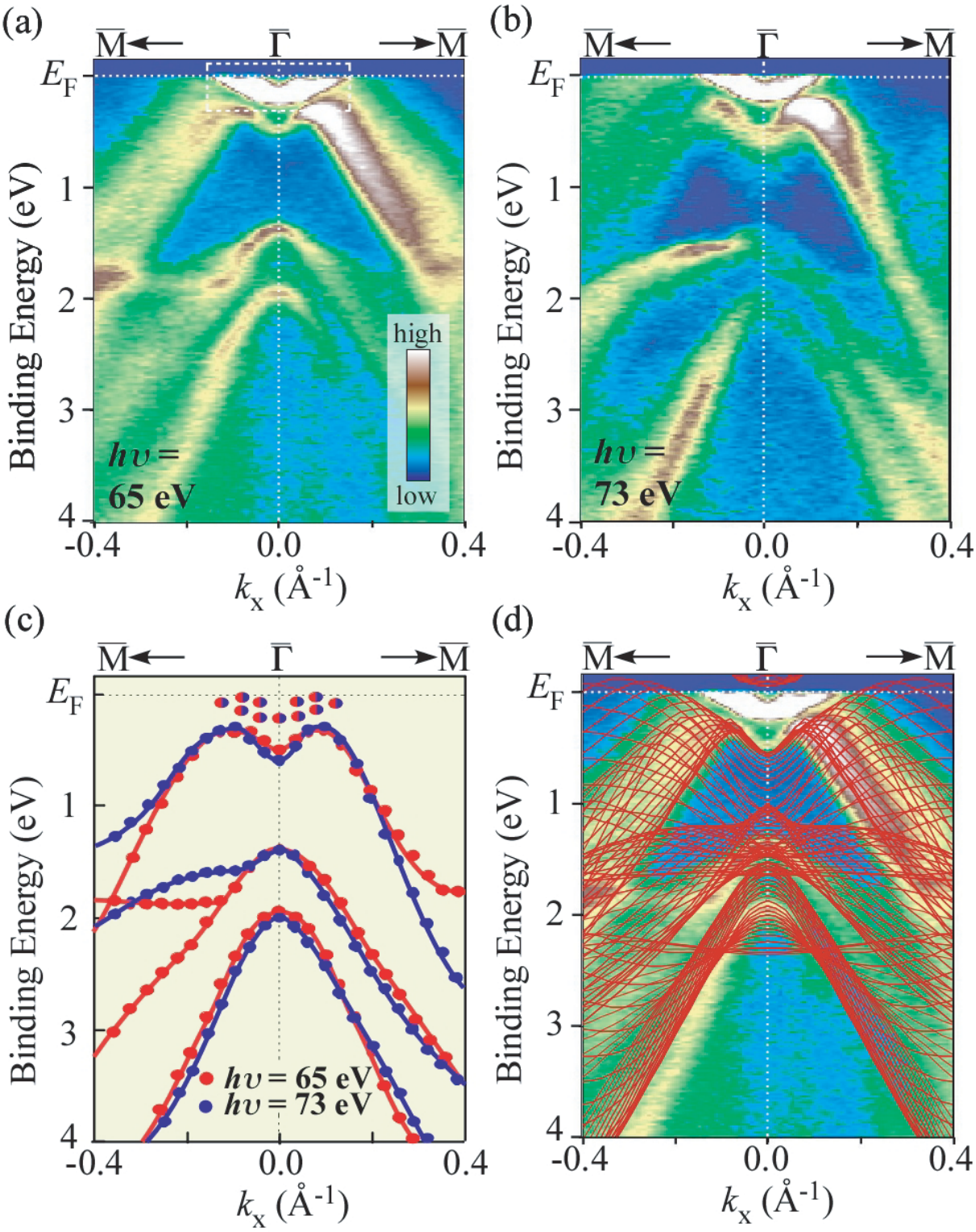

Figure 3
ARPES spectral intensity plots of Sb(111) along $\overline{\Gamma}\,\overline{M}$ direction as a function of momentum and binding energy for (a) hυ = 65 eV and (b) hυ = 73 eV. (c) Comparison of peak position between the data at hυ = 65 (red dots) eV and hυ = 73 eV (blue dots). (d) Same as (a) with the calculated bands (red lines) projected on the (111) plane.

resolution and show the results in Fig. 4, where we find that the surface band consists of two well-separated bands which share a common band bottom at $\overline{\Gamma}$ point. As shown in the inset, these two bands form characteristic anisotropic Fermi surfaces; a small hexagonal electron pocket centered at $\overline{\Gamma}$ point and six ellipsoidal hole pockets surrounding the electron pocket at $\overline{\Gamma}$ point. Next we discuss the origin of the surface bands. Since the space-inversion symmetry breaks at the surface, the degeneracy of bands due to the spin is lifted except for $\overline{\Gamma}$ point at the surface [8]. Considering this, we assign the two surface bands as the spin-split surface bands due to the spin-orbit coupling at Sb(111) surface. The observed strong anisotropy of Fermi surfaces demonstrates that the spin-orbit interaction is quite anisotropic. The present ARPES study clearly indicates that the

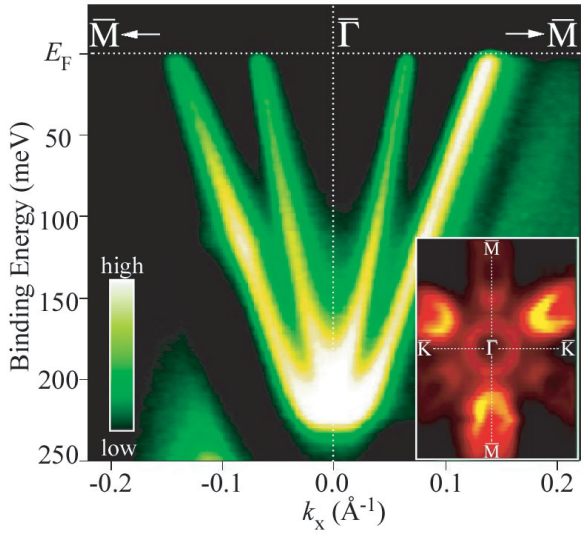

Figure 4
ARPES spectral intensity plot near E_F of Sb(111) around $\bar{\Gamma}$ point as a function of momentum and binding energy. Inset shows the intensity plot at E_F as a function of two-dimensional momentum.

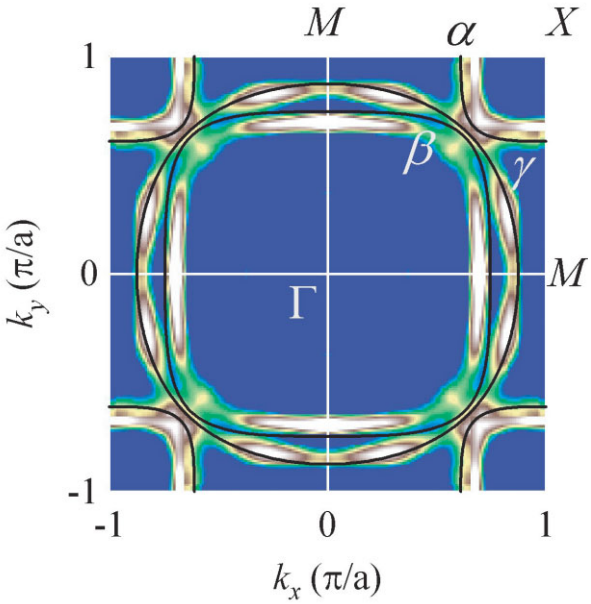

Figure 5
E_F intensity map of monolayer ruthenate Sr_2RuO_4 recorded with a photon energy of 65 eV at 30 K. The white lines denote the Fermi surfaces of the LDA calculation.

anisotropic spin-orbit coupling characterizes the surface electronic structure of group-V semimetals and probably account for reported peculiar physical properties such as granular superconductivity.

K. Sugawara[1], T. Sato[1], S. Souma[1], T. Takahashi[1], M. Arai[2], T. Sasaki[2], M. Kubota[3] and K. Ono[3] ([1]Tohoku Univ., [2]NIMS, [3]KEK-PF)

References

[1] C. A. Hoffman, J. R. Meyer, F. J. Bartoli, A. Di Venere, X. J. Yi, C. L. Hou, H. C. Wang, J. B. Ketterson and G. K. Wong, *Phys. Rev. B*, **48** (1993) 11431.
[2] B. Weitzel and H. Micklitz, *Phys. Rev. Lett.*, **66** (1991) 385.
[3] C. R. Ast and H. Höchst, *Phys. Rev. Lett.*, **87** (2001) 177602.
[4] C. R. Ast and H. Höchst, *Phys. Rev. B*, **67** (2003) 113102.
[5] C. R. Ast and H. Höchst, *Phys. Rev. Lett.*, **90** (2003) 016403.
[6] Y. M. Koroteev, G. Bihlmayer, J. E. Gayone, E. V. Chulkov, S. Blügel, P. M. Echenique and Ph. Hofmann, *Phys. Rev. Lett.*, **93** (2004) 046403.
[7] K. Sugawara, T. Sato, S. Souma, T. Takahashi, M. Arai and T. Sasaki, *Phys. Rev. Lett.*, **96** (2006) 046411.
[8] S. LaShell, B. A. McDougall, and E. Jensen, *Phys. Rev. Lett.*, **77** (1996) 3419.

4-3 Fermi Surfaces and Kink in the Energy Dispersion of Sr_2RuO_4

In studies of high-T_c superconducting cuprates, an understanding of the many-body interactions or correlation effects which dress the electrons in low-energy excitations is significantly important. Such renormalizations of the dispersion of the electrons near the Fermi level (E_F) produce a well-known "kink" - a sudden change in the group velocity of the band dispersion. Concerning the origin of this kink, various possibilities including electronic coupling to a bosonic mode such as phonons or magnetic excitations have been discussed. Despite a large number of studies, however, general consensus on the origin of the kink has not yet been achieved. We have recently found a similar kink in layered strontium ruthenates [1], demonstrating that the kink is not peculiar to the cuprates. The layered ruthenates are isostructural to the cuprates, while the two classes of oxides show quite different electronic and magnetic properties. The near-E_F electronic structure of the layered ruthenates consists not only of the in-plane Ru 4d_{xy}-O 2p bands but also of the out-of-plane Ru 4$d_{yz,zx}$-O 2p ones, while in the cuprates the single in-plane Cu 3$d_{x^2-y^2}$-O 2p band plays a crucial role in their electronic structures.

Previous angle-resolved photoemission and de Haas-van Alphen studies revealed that the Fermi surface (FS) of monolayer ruthenate Sr_2RuO_4 has three branches; one hole sheet (α) and two electron sheets (β and γ) – a result qualitatively consistent with a band-structure calculation based on the local-density approximation (LDA), as shown in Fig. 5. We have recently found an orbital selectivity of the kink in the dispersion of the monolayer ruthenate Sr_2RuO_4 in high-resolution ARPES spectra along the high symmetry lines ΓM and MX [2]. A kink was clearly observed in the ARPES taken using BL-28A for the γ FS sheet derived from the in-plane Ru 4d_{xy} orbital, but not observed for the α and β FS sheets derived from the out-of-plane Ru 4d_{yz} and 4d_{zx} orbitals. Moreover, the magnitude of the kink of the in-plane Ru 4d_{xy} was found not to diminish strongly on departing from (0, π), in contrast to the momentum dependence of the (π, 0) kink observed in Bi2212 (see Fig. 6) [3]. In exotic superconductors like the ruthenates and the cuprates, elucidating the behavior of the kink in the electron dispersion may provide a fundamental insight into the nature of the electron-pairing mechanism.

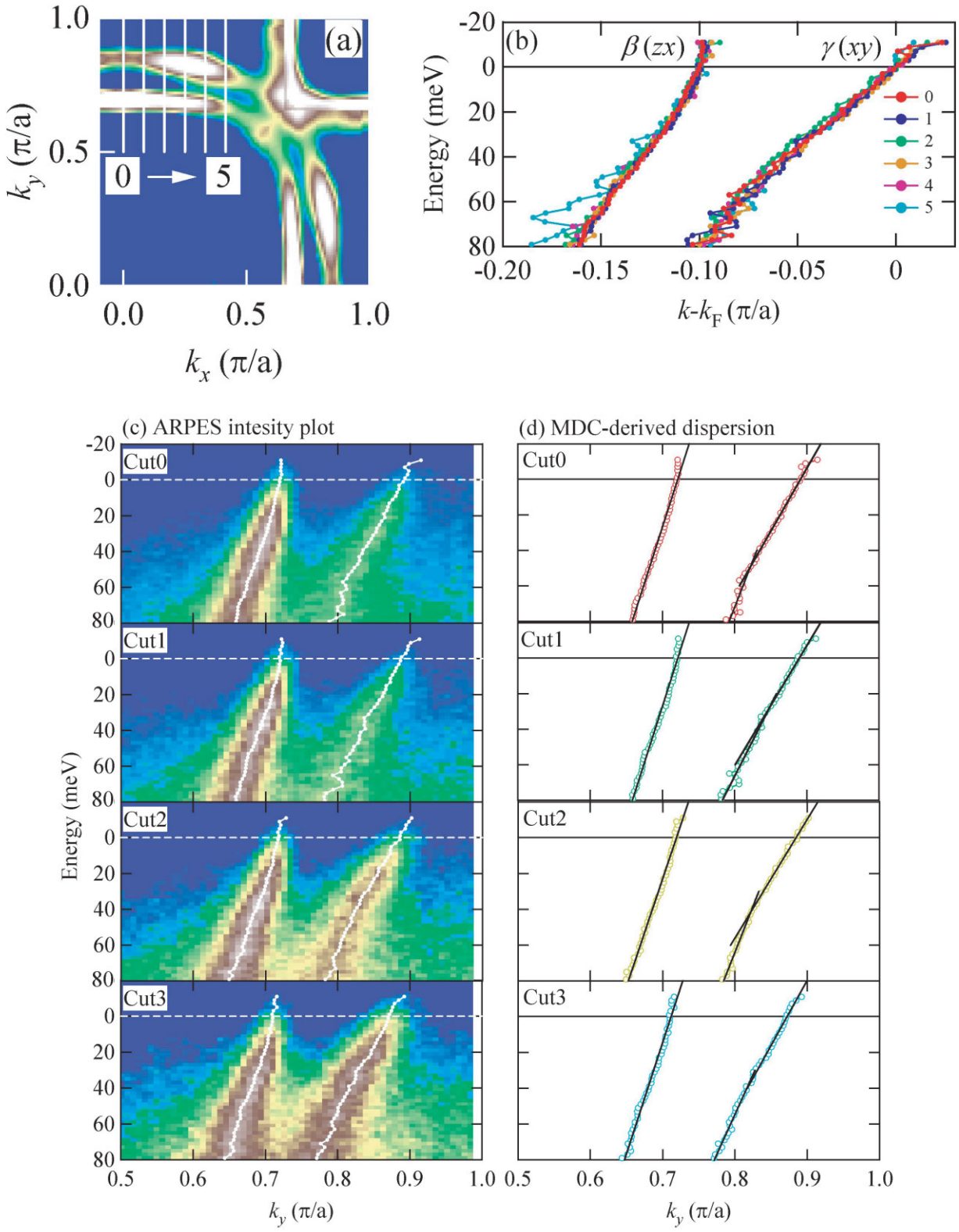

Figure 6
(a) E_F intensity map. (b) The momentum evolution of the *xy* and *zx* bands is summarized. Note that the *zx* band includes an offset of -0.1 in momentum space. (c) and (d) ARPES intensity plots and the MDC-derived dispersions of each cut. The locations of momentum cuts (0-5) are illustrated by white lines in panel (a).

Y. Aiura[1], H. Iwasawa[1,2] and T. Saitoh[2] ([1]AIST, [2]Tokyo Univ.)

References

[1] Y. Aiura, Y. Yoshida, I. Hase, S. I. Ikeda, M. Higashiguchi, X. Y. Cui, K. Shimada, H. Namatame, M. Taniguchi and H. Bando, *Phys. Rev. Lett.*, **93** (2004) 117005.
[2] H. Iwasawa, Y. Aiura, T. Saitoh, I. Hase, S. I. Ikeda, Y. Yoshida, H. Bando, M. Higashiguchi, Y. Miura, X. Y. Cui, K. Shimada, H. Namatame and M. Taniguchi, *Phys. Rev. B,* **72** (2005) 104514.
[3] H. Iwasawa, Y. Aiura, T. Saitoh, Y. Yoshida, I. Hase, S. I. Ikeda and H. Bando, *Physica C* **445-448** (2006) 73.

4-4 Band Structure and Fermi Surface of $La_{1-x}Sr_xMnO_3$ Thin Films Studied by *In-Situ* Angle-Resolved Photoemission Spectroscopy

Hole-doped perovskite manganese oxides $La_{1-x}Sr_xMnO_3$ (LSMO) have attracted considerable attention because of their interesting magnetic and electrical properties, such as colossal magnetoresistance and composition- and temperature-dependent metal-insulator transitions [1,2]. In order to clarify the origin of their physical properties, it is necessary to determine the band structure and Fermi surface (FS) of these oxides. Angle-resolved photoemission spectroscopy (ARPES) is a unique and powerful technique for experimentally determining the band structure of a solid and has long played a central role in studies of the electronic states of strongly correlated electron systems [3]. It has recently been possible to obtain well-ordered surfaces of transition-metal oxides (TMO's) using the laser molecular-beam epitaxy (laser MBE) technique. This progress has enabled studies of the band structure of TMOs with three-dimensional crystal structures by using an *in situ* ARPES system combined with a laser MBE chamber [4]. Here, we report the first observation of the band structure near the Fermi level (E_F) in LSMO and its change with the metal-insulator transition using *in situ* ARPES on laser-MBE grown well-ordered surfaces.

The clean and well-ordered surface of LSMO indispensable for ARPES measurements was confirmed by atomic force microscopy (AFM) and a low energy-electron-diffraction (LEED) characterization. Atomically-flat step-and-terrace structures in the AFM image (Fig.7(a)) and sharp 1×1 spots with some surface-reconstruction-derived spots in the LEED pattern (Fig. 7(b)) confirm the high quality of the LSMO-film surface and consequently the reliability of the ARPES spectra.

Figure 8(a) shows ARPES spectra of an LSMO (x = 0.4) thin film recorded at 25 K with a photon energy of 88 eV at BL-28A, mostly reflecting the complicated band structure along the Γ–X direction in the tetragonal

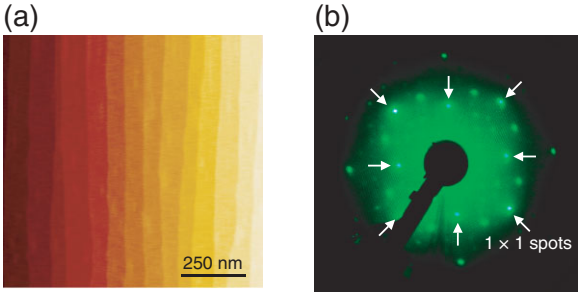

Figure 7
(a) AFM image of a 400-Å-thick $La_{0.6}Sr_{0.4}MnO_3$ film grown on a $SrTiO_3$ (001) substrate. (b) LEED pattern of the in-vacuum $La_{0.6}Sr_{0.4}MnO_3$ thin film observed with an electron energy of 100 eV. The arrows indicate the locations of the 1×1 spots.

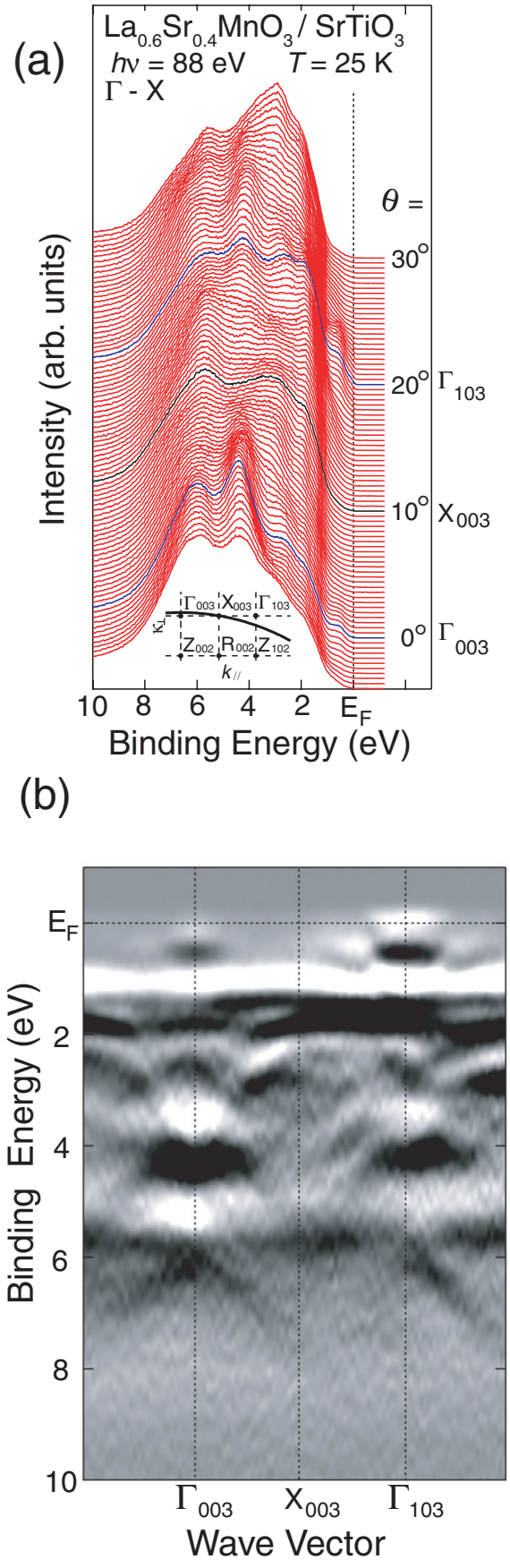

Figure 8
(a) *In situ* angle-resolved photoemission spectra along the Γ – X direction of the $La_{0.6}Sr_{0.4}MnO_3$ thin film. The corresponding path in the BZ is indicated with a thick line in the inset. The polar angle (θ) referred to the surface normal is indicated. (b) Experimentally derived band structure in the Γ – X direction of the $La_{0.6}Sr_{0.4}MnO_3$ thin film obtained from the *in situ* ARPES measurements. The dark regions correspond to the energy bands.

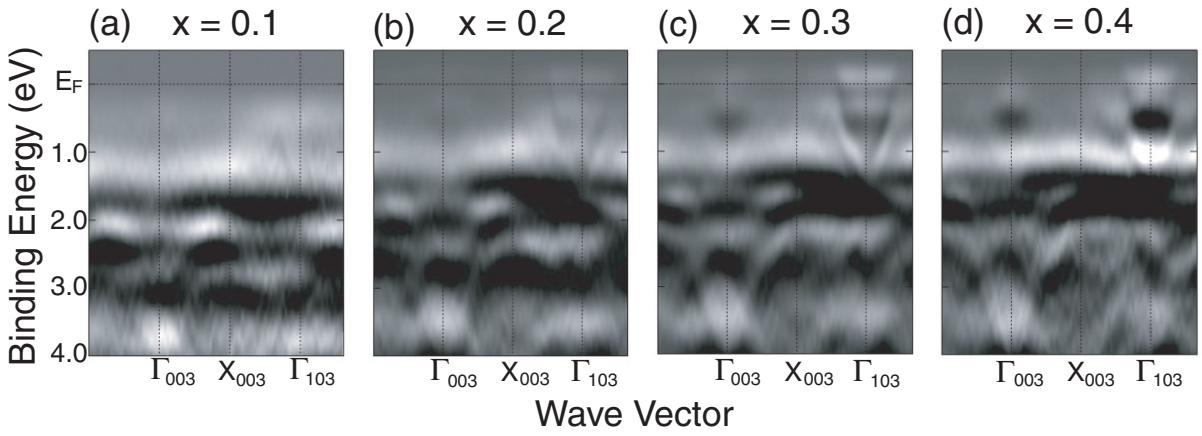

Figure 9
Experimental band structures along the Γ – X direction of $La_{1-x}Sr_xMnO_3$ ((a) $x = 0.1$, (b) $x = 0.2$, (c) $x = 0.3$, and (d) $x = 0.4$) thin films obtained from *in situ* ARPES measurements.

Brillouin-zone (BZ) [5]. The ARPES spectra exhibit considerable and systematic changes as a function of the polar angle. To see more clearly the dispersive feature of the bands in the ARPES spectra, the experimental band structure is mapped out in Fig. 8(b). The peak position of each dispersed band has been obtained by taking the second derivative of the ARPES spectra after smoothing, and plotting the intensity on a grayscale. The darkest areas of the plot correspond to the energy bands. As Fig. 8(b) shows, the band structure of the LSMO (x = 0.4) thin film consists of several highly dispersive O 2*p*-derived bands at binding energies ranging from about 2.3 eV to 6.0 eV and Mn 3*d* derived bands near E_F. Moreover, a dispersive band near E_F indicative of an electron pocket is clearly observed around the Γ point. Compared with a band-structure calculation based on the local density approximation + *U*, the estimated size of the electron Fermi surface is consistent with the prediction of the theory, while the width of the conduction band in the experiment is significantly narrower than that in the calculation. This discrepancy between experiment and theory suggests a significant renormalization effect of the Mn 3*d* band due to strong correlations [6].

Figures 9(a-d) show the experimentally derived band structures of LSMO ($x = 0.1$, 0.2, 0.3, and 0.4) thin films determined by *in situ* ARPES measurements. We have found that the electron pocket clearly observed in ferromagnetic metal LSMO ($x = 0.4$) films is gradually smeared out with decreasing hole concentration, almost disappearing at $x = 0.1$ (antiferromagnetic insulator). The anomalous behavior of the FS associated with the metal-insulator transition reflects the complicated underlying physics in LSMO with hole doping.

A. Chikamatsu, H. Kumigashira and M. Oshima (The Univ. of Tokyo)

References

[1] M. Imada, A. Fujimori and Y. Tokura, *Rev. Mod. Phys.*, **70** (1998) 1039, and references therein.
[2] J. -H. Park, E. Vescovo, H. -J. Kim, C. Kwon, R. Ramesh and T. Venkatesan, *Nature,* **392** (1998) 794.
[3] Z. -X. Shen and D. S. Dessau, *Phys. Rep.*, **253** (1995) 1.
[4] K. Horiba, H. Ohguchi, H. Kumigashira, M. Oshima, K. Ono, N. Nakagawa, M. Lippmaa, M. Kawasaki and H. Koinuma, *Rev. Sci. Instrum.*, **74** (2003) 3406.
[5] H. Wadati, T. Yoshida, A. Chikamatsu, H. Kumigashira, M. Oshima, H. Eisaki, Z.-X. Shen, T. Mizokawa and A. Fujimori, cond-mat/0603642.
[6] A. Chikamatsu, H. Wadati, H. Kumigashira, M. Oshima, A. Fujimori, N. Hamada, T. Ohnishi, M. Lippmaa, K. Ono, M. Kawasaki and H. Koinuma, *Phys. Rev. B,* **73** (2006)195105.

4-5 XAS and XMCD Studies of an Fe-Wedge(001) Layer Facing an Epitaxial MgO(001) Tunnel Barrier

A fully epitaxial Fe(001)/MgO(001)/Fe(001) layered structure is widely recognized as a novel magnetic tunnel junction (MTJ) with a high-magnetoresistance (MR) of about 180% at room temperature [1], and has potential applications as magnetoresistive random-access-memory (MRAM) or for magnetic sensors. We have recently reported [2,3] that a monatomic bcc Fe(001) layer directly facing an MgO(001) tunnel barrier, fabricated by the same procedure as used for MTJs showing extremely high MR, is not oxidized. The XMCD study also showed that the total magnetic moment of Fe 1 ML is enhanced compared with that of bulk Fe. This result indicates that the structure of the Fe(001)/MgO(001) interface has a crucial effect on the tunnel magnetoresistance (TMR); if partially oxidized FeO_x is formed at the interface, the MR ratio could be considerably reduced. To study the effect of the interface roughness on TMR, we have carried out XAS and XMCD studies of an "Fe-wedge(001) layer" facing an MgO(001) layer, obtaining magnetic moments as a function of average Fe thickness from 0 to 7 ML. In the region of very thin Fe thickness below about 2 ML, the roughness effect may be serious due to the existence of many Fe islands on the MgO(001).

We prepared a fully epitaxial multilayer with an Fe-wedge(001) (0 to 7 ML)/MgO(20 Å)/AlO(20 Å) using

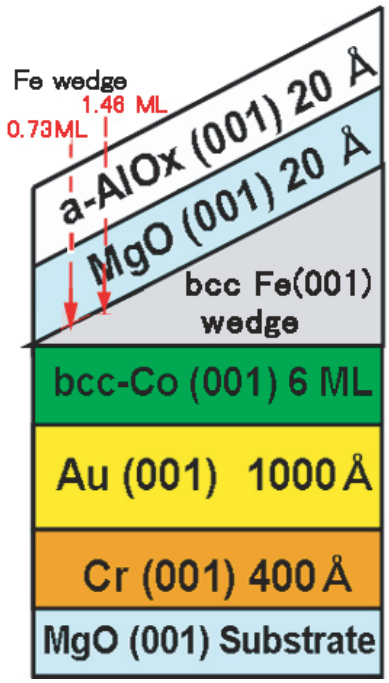

Figure 10
Structure of the Fe-wedge sample covered by MgO. Arrows show the positions of the incident beam for the XAS and XMCD spectra presented in Fig. 11. The corresponding Fe-wedge thicknesses are also given.

the molecular-beam epitaxy (MBE) method with *in-situ* RHEED observation (the structure is presented in Fig. 10). Buffer layers of MgO(001)substrate/Cr(001) (400 Å)/Au(001) (1000 Å)/bcc-Co(001) 6 ML were used. The single-crystalline MgO(20 Å) layer was grown at room temperature using electron-beam evaporation of a single-crystalline MgO source material. XAS and XMCD studies were carried out at BL-11A. Magnetic fields of 4 T were applied to the sample using an ultrahigh-vacuum superconducting magnet. Magnetic moments were evaluated using the sum rules and the energy-integrated XAS and XMCD spectra.

Figure 11 shows typical XAS spectra, XMCD spectra and XMCD integrations at the Fe $L_{2,3}$ edges of Fe-wedge(001)/MgO(20 Å) in the region of very thin average Fe thickness (0.73 and 1.46 ML, denoted by arrows in Fig. 10). No extra shoulders in the XAS spectra due to the multiplet effect in FeO_x were observed at any Fe thickness. However, the total magnetic moment of the Fe-wedge drastically decreased from 2.56 ± 0.1 μ_B to 1.87 ± 0.1 μ_B as the average Fe thickness decreased from 2 ML to 0.73 ML. Figure 12 presents the total magnetic moment as a function of the thickness of the Fe wedge. Above about 4 ML the total moment shows an almost constant value of 2.65 ± 0.1 μ_B with a spin moment of 2.52 ± 0.1 μ_B and an orbital moment of 0.13 ± 0.1 μ_B. Since the total magnetic moment for a uniform monatomic bcc-Fe(001) layer (not wedged) directly facing MgO is 2.54 ± 0.1 μ_B [2,3], the reduction of the total moment in the region below 2 ML in the present Fe-wedge can be attributed to interface roughness, possibly originating from a weak chemical bond between the edges of Fe islands and MgO.

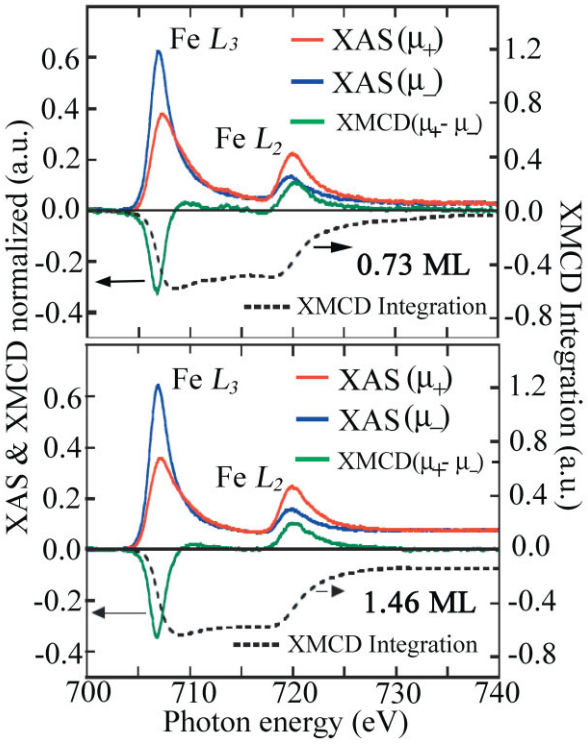

Figure 11
XAS and XMCD spectra and XMCD integrations for two thicknesses of the Fe-wedge in the MgO-covered Fe-wedge sample. Average thicknesses are 0.73 ML and 1.46 ML, denoted by arrows in Fig. 10.

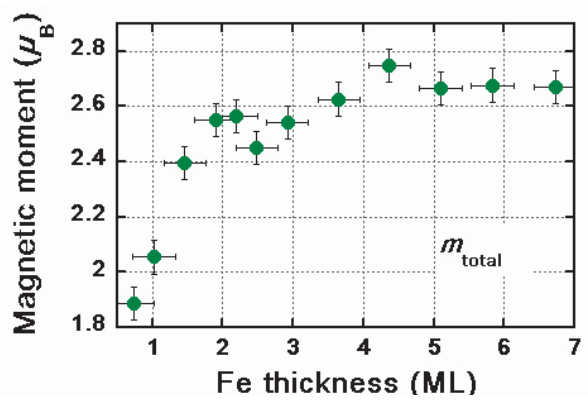

Figure 12
Total magnetic moment as a function of average Fe thickness in the MgO-covered Fe-wedge sample.

T. Saito[1], T. Katayama[1], K. Miyokawa[1], S. Saito[1], T. Kamino[1], K. Hanashima[1], Y. Asano[1], K. Mamiya[2], T. Koide[2], Y. Suzuki[3] and S. Yuasa[4,5] ([1]Toho Univ., [2]KEK-PF, [3]Osaka Univ., [4]AIST, [5]CREST-JST)

References

[1] S. Yuasa, T. Nagahama, A. Fukushima, Y. Suzuki and K. Ando, *Nature Materials,* **3** (2004) 968.
[2] K. Miyokawa, S. Saito, T. Katayama, T. Saito, T. Kamino, K. Hanashima, Y. Suzuki, K. Mamiya, T. Koide and S. Yuasa, *Jpn. J. Appl. Phys.*, **44** (2005) L9.
[3] S. Saito, K. Miyokawa, T. Katayama, S. Yuasa, T. Kamino, K. Hanashima, T. Saito, Y. Suzuki, K. Mamiya and T. Koide, *J. Magn. Soc. Jpn.*, **29** (2005) 463.